Research paper

Title: Dissection of the early pollen-stigma interactions by live-cell imaging

Authors: Frédérique Rozier[1], Lucie Riglet[1+], Chie Kodera[1$], Vincent Bayle[1], Eléonore Durand[2], Thierry Gaude[1] and Isabelle Fobis-Loisy[1*]

Author affiliation:

[1] Laboratoire Reproduction et Développement des Plantes, Univ Lyon, ENS de Lyon, UCB Lyon 1, CNRS, INRA, F-69342, Lyon, France

[+] Present address: Sainsbury Laboratory, University of Cambridge, Bateman Street, Cambridge CB2 1LR, UK

[$] Present address : Institut Jean-Pierre Bourgin, Institut National de la Recherche Agronomique (INRA), AgroParisTech, CNRS, Université Paris-Saclay, 78000 Versailles, France.

[2] CNRS, UMR 8198 Evo-Eco-Paleo, Université de Lille - Sciences et Technologies, Villeneuve d'Ascq, France

E-mail address:

Frederique.rozier@ens-lyon.fr, lucie.riglet@slcu.cam.ac.uk, Chie.Kodera@inra.fr, vincent.bayle11@ens-lyon.fr, eleonore.durand@univ-lille.fr, thierry.gaude@ens-lyon.fr, Isabelle.fobis-loisy@ens-lyon.fr

***Corresponding author:**

Isabelle Fobis-Loisy, Laboratoire Reproduction et Développement des Plantes, Univ Lyon, ENS de Lyon, UCB Lyon 1, CNRS, INRA, F-69342, Lyon, France. (33) 4 72 72 89 85. Isabelle.fobis-loisy@ens-lyon.fr

Date of submission: 6th september 2019

Seven figures. In colour online only. No table

Three Supplementary protocols. Three Supplementary tables. Six Supplementary Figures. Six Supplementary videos.

5983 words (from the introduction to the end of the acknowledgements)

Highlight: A live imaging system coupled with self-incompatible Arabidopsis lines highlight the role of stigmatic cells in controlling pollen hydration and in reacting to pollen tube intrusion by remodeling actin cytoskeleton.

Abstract: Early events occurring at the surface of the female organ are critical for plant reproduction, especially in species with a dry stigma. Following landing on the stigmatic papilla cells, the pollen rehydrates, germinates a tube, which penetrates the cell wall and grows towards the ovules to convey the male gametes to the embryo sac. In self-incompatible (SI) species within the Brassicaceae, these processes are blocked when the stigma encounters an incompatible pollen. Here, based on the generation of SI-Arabidopsis lines and by setting up a live imaging system, we showed that control of pollen hydration has a central role in pollen selectivity. The faster pollen pumps water from the papilla during an initial period of 10 minutes, the faster it germinates. Furthermore, we found that the SI barriers act to block the proper hydration of incompatible pollen and when hydration is promoted by high humidity, an additional control prevents pollen tube penetration into the stigmatic wall. In papilla cells, actin bundles focalize at the contact site with the compatible pollen but not with the incompatible one, raising the possibility that stigmatic cells react to the mechanical pressure applied by the invading growing tube.

Keywords : actin, Arabidopsis, compatible and incompatible pollinations, hydration threshold, mechanical pressure, pollen-stigma interaction.

52 **Introduction**

53 Flowers of Brassicaceae species have a dry stigma, highly discriminatory with early control of
54 pollen capture following pollination (Dickinson, 1995). The stigma consists of a dome of flask-
55 shaped epidermal cells (papillae) once pollen grains land on papillar cells, only those recognized
56 as compatible are accepted, whereas undesirable pollen grains (i.e., from unrelated species or
57 self-pollen in self-incompatible species) are rejected (reviewed in Doucet *et al.* 2016). Pollen
58 grains need to hydrate on the stigma so as to permit the emergence of a pollen tube that
59 penetrates the papilla cell wall and then grows within the pistil tissues (reviewed in Chapman
60 and Goring 2010). *In vitro* assays showed that growing through the stigma is required for pollen
61 tubes to efficiently target the ovules (Palanivelu and Preuss, 2006). Likewise, genetic ablation of
62 the stigmatic papillae prevents normal pollen hydration or germination (Tung *et al.*, 2005). Early
63 events of the pollen-stigma interaction are thus crucial steps for successful fertilization.
64 Most of the Brassicaceae species have a self-incompatibility (SI) system, which allows the stigma
65 to reject self-pollen grains and hence to prevent self-fertilization (de Nettancourt, 2001). This
66 self/non-self recognition mechanism is genetically controlled by a single multiallelic locus, the *S*-
67 locus, and depends on a receptor-ligand interaction (Ivanov *et al.*, 2010). The ligand, the *S*-locus
68 Cysteine Rich protein (SCR/SP11), is present in the material contained in the cavities of the
69 pollen cell wall (Schopfer *et al.*, 1999; Takayama *et al.*, 2000), migrates to the papilla surface and
70 interacts with the *S*-locus Receptor Kinase (SRK) (Stein *et al.*, 1991), localized to the plasma
71 membrane of stigmatic papillae. This interaction induces SRK phosphorylation and activation of
72 the signaling cascade leading to self-pollen rejection (Cabrillac *et al.*, 2001). Incompatible pollen
73 grains fail to hydrate properly and do not germinate or only germinate a short pollen tube
74 whose growth is arrested on papilla cells (Dickinson, 1995; Hiroi *et al.*, 2013). Although
75 *Arabidopsis thaliana* is self-fertile, transgenic SI *A. thaliana* lines were generated by
76 reintroducing SCR/SP11 and SRK gene pairs from its SI close relative *A. lyrata* (Nasrallah and
77 Nasrallah, 2002; Nasrallah *et al.*, 2004). SI Arabidopsis lines have opened the way for thorough
78 analysis of pollen-stigma recognition mechanisms through the use of the genetic tools and
79 mutant collections available for this model plant species.

80 Although they have been studied for many years, the early steps leading to pollen acceptance or
81 rejection decision are still not clearly characterized. In this work, based on the generation of
82 new SI Arabidopsis lines, we revisited the cellular aspects of pollen-stigma interaction by setting
83 up a live imaging system to monitor pollen hydration and germination following compatible as
84 well as incompatible pollinations. We quantified the degree of pollen hydration required for
85 pollen activation and highlighted a late SI control restricting penetration of stigmatic cell wall by
86 the pollen tube. Furthermore, we monitored the dynamics of actin network during compatible
87 and incompatible pollination and found that remodeling of actin cables is triggered in stigmatic
88 cells only when pollen-stigma interaction is engaged in compatibility.
89
90 **Materials and methods**
91
92 **Plant growth conditions**
93 *A. thaliana* Col-0, C24, *A. lyrata ssp petraea* haplotype *S14* originating from the Czech Republic
94 (seeds kindly provided by Dr Pierre Saumitou-Laprade, Université de Lille F59655 Villeneuve
95 d'Ascq cedex, France) and all transgenic plants were grown in growth chambers under a long-
96 day cycle of 16-h light/8-h dark at 21°C/19°C with a relative humidity around 60 %. *A. lyrata*
97 plants were propagated by cuttings every 3 months.
98
99 ***A. lyrata SCR14* and *SRK14* gene cloning, plasmid construction, plant transformation and gene**
100 **expression**
101 The *AlSRK14* genomic sequence spanning the coding region from the start to the stop codons
102 (3,620 kb) and a fragment of 4,081 kb containing the *AlSCR14* gene, 1,844 kb of the 5' upstream
103 region and 817 bp of the 3' downstream region were amplified from genomic DNA of *A. lyrata*
104 containing the *S14* locus. Subsequent clonage steps and transgenic lines produced in this work
105 are described in Supplementary protocol S1. Sequences of *AlSRK14* and *AlSCR14* transgenes
106 introduced in *A. thaliana* have been submitted to GENBANK (*pSLR1-gAlSRK14*: accession
107 number MH680585, *pgAlSCR14*: accession number MH680584).

108 *AlSRK14* expression level in stigma of transgenic plants was determined as described in
109 Supplementary protocol S2.
110
111 **Pollination assays**
112 Flower buds at the end of developmental stage 12 (Smyth *et al.*, 1990) were emasculated and
113 18 hours later stigmas that had reached developmental stage 13 or Early 14 (14E) were
114 manually pollinated on plant with mature pollen. Six hours after pollination, stigmas were fixed
115 in acetic acid 10 %, ethanol 50 % (v/v) and stained with aniline Blue (Kho and Baër, 1968) for
116 pollen tube counting. In a second series of pollination assay, stage 12 flower buds were
117 emasculated and 42h (stage 15) or 66 h (stage 16) later, stigmas were pollinated with fresh
118 mature pollen followed by fixation and aniline blue staining. In a third experiment, stigmas were
119 pollinated at stage 13-14E and collected after six, 24, 48 or 72 hours followed by fixation and
120 aniline blue staining. Pollination assays were carried out on at least three stigmas and repeated
121 at least at two different dates. Pollination was considered as incompatible when less than five
122 pollen tubes were counted in the stigma (Kitashiba *et al.*, 2011).
123
124 **Dual pollination: semi *in vivo* assay**
125 Stage 12 flower bud was emasculated and 18 hours later (stage 13-14E), pistil was cut
126 transversally in the middle of the ovary and placed vertically in a half-cut, perforated PCR tube
127 whose base was introduced in a solid agar medium. Pollen was deposited by gently touching the
128 stigma with a mature anther. Incompatible pollen was deposited first, followed (within less than
129 1 min) by deposition of compatible pollen, which defined the timing starting point (T0) for
130 monitoring pollen behavior. A cover slip was delicately applied on the surface of the pollinated
131 stigma for confocal imaging. The system was maintained throughout the experiment at 21°C
132 and under 45 % relative humidity. To increase the relative humidity at the vicinity of the
133 pollinated stigma, pieces of solid agar medium were added around the mounted pistil. For cell
134 surface labelling, after 35 minutes in high humidity conditions, pollinated stigma was incubated
135 in FM™ 4-64 Dye (*N*-3-Triethylammoniumpropyl-4-6-4-Diethylamino Phenyl Hexatrienyl
136 Pyridinium Dibromide, Life Technologies T3166, 8.23 μM) for five minutes and subsequently

137 washed in 1/2 Murashige and Skoog basal medium containing 10 % (w/v) of sucrose, before
138 mounting between slide and coverslip in this medium.
139
140 **Confocal Microscopy and Fluorescence quantification at the contact point with the**
141 **incompatible pollen**
142 Images were acquired with a SP8 laser-scanning confocal microscope (Leica) using a 25x
143 objective (numeric aperture 0.95, water immersion). Detailed acquisition settings are provided
144 in Supplementary protocol S3. Fluorescence at the contact point with the incompatible pollen
145 was quantified as described in Supplementary protocol S3.
146
147 **Measurement of pollen hydration rate**
148 Because the increase of water content in pollen grain is correlated with change of its shape
149 from ellipsoid to spheroid (Zuberi and Dickinson, 1985; Hiroi *et al.*, 2013; Wang *et al.*, 2016), for
150 each pollen grain, we recorded every two minutes the ratio between the long and the wide axis
151 (L/W) to estimate the pollen hydration rate until germination. Slopes were determined by linear
152 regression of the hydration curve based on pollen ratio evolution during the first 10 minutes
153 period (5 data points), using the curve $f = ax + b$.
154
155 **Seed set**
156 Flower buds at stage 12 were emasculated and pollinated with mature pollen 18 h later. 21 days
157 after pollination, mature siliques were opened to count the number of seeds.
158
159 **Statistic analysis**
160 For each experiment (except the initial selection of SRK and SCR transgenic plants), at least two
161 independent biological replicates (performed at different dates) were carried out. After
162 checking that the mean and variability of the samples were homogenous between replicates,
163 data were pooled to apply a statistical test. Graph and statistics were obtained with R studio or
164 Excel softwares. We tested the sample distribution with a Shapiro-Wilk test and applied a
165 Student-test to compare the mean of two given data sets. To compare multiple samples with a

166 single test, we performed an ANOVA. In this study, p-values < 0.05 were considered statistically
167 significant.
168
169 **Results**
170
171 **Generation of transgenic lines designed for live cell imaging**
172 We generated transgenic plants for *AlSRK14* in Col-0 background as this accession is more
173 suitable for crossing with available fluorescent marker lines. We used the *Brassica oleracea SLR1*
174 (*S-locus-related gene 1*) promoter to express the *Al*SRK14 receptor in stigmatic cells. Among the
175 12 transgenic lines we generated, we isolated four independent lines possessing a unique
176 insertion and homozygous for *AlSRK14*. Stage 13-14E stigmas from these four lines rejected
177 pollen from the original *A. lyrata S14* plant (less than five pollen tubes/stigma) whereas *A. lyrata*
178 pollen produced numerous pollen tubes on Col-0 stigmas (Supplementary Fig S1A, B, C). We
179 quantified the expression level of the *AlSRK14* transgene in stage 13-14E stigmas of the two
180 strongest transgenic plants (lines #10 and #18, Supplementary protocol S2) and found that the
181 relative expression was two times lower than that detected in *A. lyrata S14* stigmas but still
182 sufficient to induce SI response (Supplementary Fig S1D). We selected the transgenic line #10
183 for further analysis and named it Col-0/*AlSRK14.* In spite of several attempts to introduce
184 *AlSCR14* in Col-0, we did not succeed in generating transgenic pollen that could be rejected by
185 stigmas of Col-0/*AlSRK14*. As an alternative, we used the C24 accession, this accession exhibiting
186 a strong SI response when transformed with *A. lyrata SRK*/*SCR* genes (Nasrallah et al., 2004; Liu
187 et al., 2007). We first transformed C24 plants with *AlSRK14* to generate a female tester capable
188 of rejecting *A. lyrata S14* pollen grains (named C24/*AlSRK14* line #14; Supplementary Fig S1C).
189 Then, among the 18 transgenic lines transformed with *AlSCR14* in C24 background, we isolated
190 five independent lines with unique insertion and homozygous for *AlSCR14*. Pollen from each of
191 these lines was rejected on C24/*AlSRK14* line #14 mature stigmas (Supplementary Fig S1E). We
192 selected transgenic line #4 for further analysis, which was named C24/*AlSCR14.*
193 To facilitate live-cell monitoring of pollen tube growth on the stigma, we introduced Lifeact
194 fused to Venus to label stigma papillae of Col-0/*AlSRK14 (*Col-0/SRK14 + Act:Venus), TURQUOISE

195 protein to monitor compatible pollen of C24 (C24/TURQ) and RFP for incompatible pollen of
196 C24/*AlSCR14* (C24/SCR14 + RFP) (Fig. 1A). We found that the presence of fluorescent proteins
197 did not alter the compatibility (ANOVA test p-value = 0.23), as well as the SI response (T-test p-
198 value = 0.15) assessed by pollen tube counting (Fig. 1B). Despite the strong pollen rejection
199 response following incompatible cross (Col-0/SRK14 + Act:Venus x C24/SCR14 + RFP), some
200 seeds developed in siliques (Fig. 1C). A comparable number of seeds were counted in siliques
201 derived from an incompatible cross between non-labeled pollen and stigmas (mean values of
202 18.35 versus 19.04, T-test p-value = 0.82, Fig. 1C). However, the incompatible crosses exhibited
203 a significantly reduced seed set compared with the compatible ones (T-test p-value = 2.2E-16
204 between the four compatible crosses cumulated and the two incompatible crosses cumulated,
205 Fig. 1C). Together, our data show that we succeeded in restoring SI system in *A.thaliana* using a
206 new *A. lyrata* haplotype *S14* and that a mature stigma recognizes and rejects incompatible
207 pollen independently of the accession background. Futhermore, expressing a fluorescent
208 protein in addition to the SI determinant does not modify completion of the SI response.
209
210 **SI response is maintained for about two days and then partially breaks down**
211 As some seeds could develop in siliques following incompatible crosses (Fig. 1C), we
212 investigated how persistent the SI response was during stigma development. To this end, we
213 first carried out pollination experiments using compatible (C24/TURQ) or incompatible
214 (C24/*AlSCR14*) pollen grains deposited on Col-0/SRK14 + Act:Venus stigmas at different pistil
215 developmental stages (Fig. 2A). When incompatible pollen grains were deposited on stage-15
216 stigmas, almost no pollen tube bypassed the stigmatic barrier (mean of 1.85 tube/stigma, graph
217 Fig. 2A), whereas some pollen tubes succeeded in penetrating stage-16 stigmas (mean of 13.2
218 tubes/stigma, graph Fig. 2A). By contrast, when compatible pollinations were performed on
219 stigmas at stages 15 or 16, pollen tubes abundantly grew in the stigma. In a second set of
220 experiments, we examined how long incompatible pollen grains deposited on stage 13-14E
221 stigmas could stay inhibited after 6, 24, 48 or 72 hours of contact with papilla cells (Fig. 2B). We
222 observed a breakdown of the SI barrier 48h and 72h after pollen deposition, when stigmas
223 reached stage 16 and stage 17, respectively. However, the number of pollen tubes overpassing
224 SI barrier (mean of 9.9 tubes/stigma and 7.3 tubes/stigma, respectively, graph Fig. 2B) was

225 much less than the massive invasion observed in compatible situations (on average more than
226 50 tubes/stigma, graphs Fig. 2A, B). Together, these experiments show that partial breakdown
227 of the SI response occurs late during pistil ageing and that a strong SI phenotype is maintained
228 during a large time-window of floral development, from stage 13 (anthesis) to stage 15 (stigma
229 extended above long anthers), that is to say slightly less than two days (Smyth *et al.*, 1990). Thus
230 the SI pollination partners we generated are suitable for developing a live-cell imaging to
231 monitore pollen behavior at the surface of mature stigmas (stage 13-14E) without risking
232 weakening of the SI barrier.
233
234 **Design of a semi *in vivo* assay that allows live cell imaging of early pollination events**
235 To study the very early cellular changes that occur following pollen-stigma interaction, we
236 designed a device that maintains stigma alive for at least one hour and allows cell-live imaging
237 under confocal microscopy (Fig 3A). In this system, compatible and incompatible pollen can be
238 separatly deposited on the same stigma and their behavior tracked in the same experimental
239 conditions (Fig 3B, Supplementary video S1). To test whether this device permitted the
240 maintenance of compatibility/incompatibility responses, we performed five independent
241 experiments where a Col0/SRK14+Act:Venus stigma was dual-pollinated with C24/SCR14+RFP
242 (incompatible) and C24/TURQ (compatible) pollen grains. We found that the percentage of
243 germination for compatible pollen varied from 58 % to 81 %, with a mean value of 74 % (n=106,
244 Fig. 3C). Emission of a pollen tube occurred on average 20 minutes after pollen deposition (Fig.
245 3C). On the contrary, germination of incompatible pollen was a rare event, occurring for only 1.3
246 % of the tracked grains (n=75, Fig. 3C). Thus, our semi *in vivo* system allows live cell imaging of
247 pollinated stigmas while preserving the highly regulated SI process.
248
249 **Actin dynamics in stigmatic cells during pollination**
250 Because remodeling of the actin cytoskeleton in the papilla cells has been reported following
251 pollination in Brassica (Iwano *et al.*, 2007), we decided to monitor actin dynamics over time.
252 Before pollination, we found the actin cytoskeleton network to be composed of bundles mainly
253 oriented along the longitudinal axis of the stigmatic cell (Fig. 4A). Upon compatible pollination, a

254 clear accumulation of actin that focalized at the contact site with the compatible pollen was
255 observed in 92 % of the pollinated papillae (22/24, Fig. 4B). For 25% the stigmatic cells (6/24),
256 actin fluorescence increased beneath the pollen grain just before appereance of a protusion at
257 the periphery of the grain corresponding to the pollen tube emergence site (deformation). For
258 17% of the stigmatic cells (4/24), actin accumulation appeared during pollen deformation. For
259 50% of the cell, actin focalized when a clear emergence of the tube (minimum 1 μm) was visible
260 (8%, 2/24) or when the tube started to grow on the stigma surface (42%, 10/24, Fig. 4C,
261 Supplementary video S2). At later stages of pollen tube progression, actin focalization was
262 observed all along the tube path in 83% (20/24) of the monitored papilla cells (Fig. 4D,
263 Supplementary video S3). Interestingly, when several pollen germinated on the same papilla,
264 actin focalization was observed below each tube (Fig.4E). By contrast, on the seven dual-
265 pollinated stigmas we tracked over time, we never detected any actin focalization beneath the
266 incompatible pollen grains (Supplementary video S4). All together, our live-cell imaging analysis
267 shows that the actin cytoskeleton polymerizes in the stigmatic cell following deposition of
268 compatible but not incompatible pollen grains. Actin accumulation starts at the pollen contact
269 site just before pollen deformation and goes on throughout the elongation of the pollen tube.
270

271 **Kinetics of compatible pollen hydration is divided into two phases**

272 Next, we compared the kinetics of pollen hydration and germination following dual pollination,
273 using the L/W ratio as a proxy for pollen hydration (Zuberi and Dickinson, 1985). At maturity,
274 the mean L/W ratio of pollen grains was close to two (Fig. 5A, Supplementary table S1). We
275 measured the pollen ratio every two minutes, starting two minutes after pollen deposition (Fig.
276 5B, Supplementary Fig S2). Among the 69 compatible pollen grains we tracked, 58 germinated in
277 the course of the experiment whereas 11 never did. We found that during the first 10 minutes
278 (preceding germination, Supplementary table S2), the mean pollen ratio dramatically decreased
279 indicating that grains were taking up water and got roundish (solid blue curve Fig. 5B). Water
280 uptake continued during the following 20 minutes, but at a much slower rate as the hydration
281 curve gets flatter. We found that germination started when the pollen ratio was below 1.4 (solid
282 blue curve Fig. 5B). Among the 58 pollen grains that germinated during the course of the

experiment, a huge majority (57/58) reached the 1.4 ratio before germination; only one germinated pollen grain never reached this ratio. For the 11 compatible pollen grains that never germinated (dashed blue curve Fig. 5B), the hydration curve shows no rapid hydration phase during the first 10 minutes and the mean ratio never reached the value of 1.4. Taken together, our results show that in Arabidopsis, water transport toward the pollen grain follows a bi-phasic kinetics: first, an initial phase characterized by a high pollen hydration rate required to reach a certain degree of water content in the pollen (ratio 1.4), followed by a second phase where the hydration rate dramatically decreases and pollen germination occurs.

Variability in pollen germination time depends on the hydration rate during the early interaction phase

In our experimental conditions, pollen germination was not synchronous, starting 12 minutes after pollen contact with the stigma and spreading over the 32 min of the experiment (Supplementary table S2). We suspected that different hydration rates of pollen grains might be the cause of this variability. To test this hypothesis, we classified the 69 compatible pollen grains according to their germination capability and categorized them into four classes: those that germinated early (from 12 to 18 minutes, n = 19), with an intermediate time (from 20 to 24 minutes, n = 22), late (from 26 to 32 minutes, n = 17), and those that did not germinate (n = 11), and we compared their hydration rate during the rapid hydration phase from two to 10 min (Fig. 5C). At two min, no significant differences were found between the L/W ratios of pollen for each classes (1.85/1.87/1.85/1.96, respectively; ANOVA test p-value = 0.13, Fig. 5C). At 10 min, pollen that germinated late were significantly less hydrated (higher L/W ratio) than those that germinated early or with an intermediate time (T-test p-value = 2.43E-04 and 1.64E-03, respectively, Fig. 5C), though their hydration degree was significantly higher than non germinated pollen (T-test p-value = 3.62E-02, Fig. 5C). We calculated the slopes of the hydration curves by linear regression, as previously described (Wang *et al.*, 2016), and found that early and intermediate germinating pollen grains had the highest hydration rates compared with late and non germinating pollen grains (Fig 5C). Non germinating pollen exhibited a very slow hydration rate (slope - 0.043) associated with a poor water uptake at 10 min, deduced from the

312 high pollen ratio (mean of 1.77). Our data show that most of the tracked compatible pollen
313 germinated within 32 minutes and that the germination time relates to the capacity of the
314 pollen to uptake water during an initial short period of 10 minutes. The faster the pollen takes
315 water from the stigma, the quicker it germinates.
316
317 **Incompatible pollen does not fully hydrate and pollen tube does not penetrate the stigmatic**
318 **cell wall**
319 Next, we examined the hydration rate of incompatible pollen on the dual-pollinated stigmas. Of
320 the 53 incompatible grains we monitored, none germinated during the time course of the
321 experiment. Futhermore, most of them (n = 43) never exhibited a L/W ratio below the threshold
322 value of 1.4 (solid red line, Fig. 6A) and only poorly hydrated compared with compatible grains
323 (solid blue curve, Fig. 6A). The mean hydration curve showed a constant slope during the 32
324 minutes of the experiment. By contrast, the 10 remaining incompatible grains had a L/W ratio
325 below 1.4 with a mean hydration curve (dashed red line, Fig. 6A) resembling that of compatible
326 pollen. In addition, their hydration rate within the first 10 minutes was similar to late
327 germinating compatible pollen (slope value of - 0.074 versus - 0.089, respectively, Fig. 6B), and
328 hence hydrated as efficiently as some compatible grains.
329 As high humidity can stimulate pollen hydration and promote incompatible pollen germination
330 (Carter and McNeilly, 1976; Ockendon, 1978; Zuberi and Dickinson, 1985), we checked the
331 effect of high humidity (100 %) on pollen behavior in a modified semi *in vivo* system
332 (Supplementary Fig S3). We found that compatible pollen germination was slightly stimulated
333 compared with standard conditions (88 % germination versus 74 % and mean germination time
334 of 18.55 minutes versus 20.38 minutes, respectively; Supplementary Fig S4). Moreover, high
335 humidity conditions did not dramatically affect actin reorganization as we detected a clear
336 focalization of actin beneath the pollen grain/tube in 75 % of the pollinated papillae (33/44)
337 (Fig. 7A, Supplementary Fig S4, Supplementary video S5). Following incompatible pollination, we
338 observed that germination of incompatible pollen was strongly stimulated, varying from 18 % to
339 58 % depending on the experiment (mean of 35 %, Supplementary Fig S5) compared with the
340 1.3 % of germination in standard conditions. In addition, among the 46 grains monitored, 46 %

341 reached a L/W ratio of 1.4 within 10 minutes (Supplementary table S3), whereas only 4 %
342 reached this value in standard conditions. However, it took more time for the incompatible
343 pollen tube to emerge (24.87 min versus 18.55 min, Supplementary Fig S5), and the tube
344 exhibited an enlarged tip and seemed blocked at the papilla surface, the pollen being detached
345 from the papilla (Fig. 7B, Supplementary video S6). The growth rate of incompatible tube was
346 1.05 μm/min, whereas a compatible tube extended much more rapidly in both standard and
347 high humidity conditions (2.41 μm/min and 1.91 μm/min, respectively, Fig. 7C). Growth kinetics
348 shows that during the first three minutes, elongation rate of both compatible and incompatible
349 tubes was comparable, but then compatible tubes extended rapidly whereas incompatible
350 tubes slowed down (Fig. 7C). These observations suggest that the incompatible tube may not be
351 able to penetrate the papilla cell wall. To test this hypothesis, we stained papilla cells with the
352 amphiphilic styryl dye FM4-64. Contrary to most plant cells where the dye labels the plasma
353 membrane (PM) and the vesicular network (Grebe *et al.*, 2003; Jaillais *et al.*, 2007; Jelínková *et*
354 *al.*, 2010), we noticed that it remained at the surface of the papilla as it did not colocalize with
355 the actin or the PM canonical marker LTI6b (Supplementary Fig S6). This labelling is probably
356 due to the interaction of the dye with the hydrophobic cuticle layer of the stigmatic cell. While
357 the compatible pollen tube clearly penetrated the FM4-64-labeled layer and grew in close
358 contact with the papilla cytoplasm identified by the actin fluorescence (9 tubes/9, Fig 7D), the
359 incompatible tube was never observed under the FM4-64 layer and stayed outside the papilla
360 (11 tubes/11, Fig 7D). Additionally, at the contact site with the short abnormal incompatible
361 tube, we rarely observed focalization of actin in the papilla, contrary to the compatible situation
362 (Fig. 7B, Supplementary Fig S5 and video S6). Taken together, our results show that
363 incompatible grains generally fail to fully hydrate, and when pollen hydration and germination
364 are promoted by high relative humidity, the SI reaction efficiently blocks tube penetration into
365 the papilla cell wall, the tube remaining outside the papilla surface without triggering actin
366 focalization at the contact site with the stigmatic cell.
367
368 **Discussion**

369 Here, we set up a live imaging system with a fast-scanning confocal microscope to
370 simultaneously monitor compatible and incompatible Arabidopsis pollen behavior on the same
371 single stigma and provide a thorough analysis of the dynamics of the cellular events following
372 pollen perception.
373
374 ***AlSCR14* and *AlSRK14* SI Arabidopsis lines**
375 The two Arabidopsis lines we generated, one that expressed the female determinant (*Al*SRK14)
376 and the second the male determinant (*Al*SCR14) were self-fertile but exhibited a strong SI
377 response when crossed. This SI response was maintained during flower development for about
378 two days, only weakening at late stages of stigma development where few pollen tubes
379 developed in pistil tissues and ultimately leading to seed set. Nevertheless, the seed yield
380 remained much below the one reported for selfed Col-0 Arabidopsis (19 seeds per silique versus
381 62 seeds per silique). Thus, these SRK14 and SCR14 transformants almost fully recapitulate the
382 SI phenotype of the natural SI Brassicaceae, the strength of the response being however less
383 persistent compared with strictly SI lines. Previous work reported a strong SI phenotype,
384 although over a narrow window, in stigmas at stage 13 and early stage 14 in Col-0 lines
385 expressing the cognate *A. lyr*ata *SCRb-SRKb* gene pair (the so-called Col-0/*AlSb* line), whereas
386 older flowers fully accepted self-pollen (Nasrallah, 2002; Nasrallah *et al.*, 2004). By contrast, in
387 another study, the same *SCRb-SRKb* gene pair was shown to be unable to confer SI in Col-0,
388 even in stage-13 flowers, the transgenic plants being fully fertile with a seed set similar to selfed
389 Col-0 plants (Indriolo *et al.*, 2014). In this latter study, a role for the E3-ubiquitin ligase ARC1 in
390 promoting SI was demonstrated as only Col-0 co-expressing the *A. lyrata* or *B. oleracea* ARC1
391 with the *SCRb-SRKb* pair acquired the capacity to reject self-pollen. Interestingly, the Col-
392 0/*AlSRK14* lines generated in our study express a strong SI response in mature stigmas without
393 the need of co-expressing *AlARC1*, the stigmas remaining partially self-incompatible at later
394 flower developmental stages. Earlier work showed that the variability of SI phenotypes
395 observed between Arabidopsis transformants was mainly due to *SRK* transcript levels (Nasrallah
396 and Nasrallah, 2014). It has been reported that transient SI phenotype and self-fertility of Col-
397 0/*AlSb* transformants were caused by modifier loci harbored in the Col-0 genome (Liu *et al.*,

398 2007; Boggs *et al.*, 2009). One of these loci, *PUB8*, encoding an ARM-repeat and U-box protein,
399 regulates *SRK* transcript levels and is responsible for the pseudo-self compatibility observed in
400 old flowers of Col-0/*AlSb* (Liu *et al.*, 2007). Contrary to the Col-0/*AlSb* transformants mentioned
401 above, in our study, *AlSRK14* expression was driven by the *SLR1* promoter region that does not
402 contain the *SRK* 5' and 3' regulatory sequences. As a consequence, it is likely that transcription
403 of *AlSRK14* gene and/or stability of the transcripts escape the regulation of Col-0 SI modifiers,
404 leading to the accumulation of AlSRK14 protein to a level sufficient to maintain a partial pollen
405 rejection response during flower development. The weakening of SI response we observed in
406 late developmental stages was expected as it is known that *SLR1* promoter activity is
407 developmentally regulated, decreasing with flower ageing (Lalonde *et al.*, 1989), and hence
408 leading to lower abundance of *SRK14* transcript levels.
409 Though we attempted to transform Col-0 with *AlSCR14*, we failed to obtain transformants
410 whose pollen grains were rejected on *AlSRK14*-expressing stigmas. In SI Arabidopsis species, a
411 dominance hierarchy between *SCR* alleles has been reported, which is regulated by small RNAs
412 (sRNAs) (Durand *et al.*, 2014). We may propose that the inability to introduce a functional
413 *AlSCR14* in Col-0 might reside in the presence of vestigial sRNAs targeting the recessive *AlSCR14*
414 allele, while these sRNAs would be absent in the C24 background.
415
416 **Pollen behavior**
417 We observed that around 20 minutes after interaction with the stigma papillae, the compatible
418 pollen germinates a tube, which is consistent with the germination time reported in Arabidopsis
419 after *in vivo* pollination (Kandasamy *et al.*, 1994; Iwano, 2004). Once emerged, the pollen tube
420 extends at a rate of 2.41 μm/min, which is significantly faster than tube elongation *in vitro*
421 (around 1 μm/min; Iwano *et al.*, 2004; Yang *et al.*, 2017) and consistent with growth rates
422 reported in other *in vivo* systems (Iwano, 2004; Cheung *et al.*, 2010). Futhermore, we found that
423 tube growth rate is not constant, exhibiting a slow growth phase whithin the first three minutes
424 after tube emergence, followed by a second phase of more rapid growth. A bi-phasic growth
425 kinetics was already reported for Arabidopsis pollen tube growing *in vitro*, except that the
426 timing was much longer; the transition from germination to a rapid growth phase requiring 30

427 minutes (Vogler *et al.*, 2015). While compatible pollen grains promptly achieve germination,
428 incompatible grains deposited on the same stigma, and in the close vicinity of compatible ones,
429 follow a complete different destiny. Indeed, incompatible pollen grains exhibit an extremely low
430 germination rate (1.3 %), which is in agreement with the few pollen tubes we detected after
431 aniline blue staining. Thus, our semi *in vivo* system recapitulates what happens in nature when
432 pollen from various origins lands on the same stigma, accepting compatible whereas rejecting
433 incompatible pollen grains.
434 We found that almost immediately after landing on the stigma, compatible pollen starts to
435 hydrate and within 10 minutes is almost fully hydrated. By contrast, during the same time
436 period, the L/W ratio of incompatible grains only poorly evolves. Thus, inhibition of the
437 incompatible pollen acts very early, within the first minutes following stigma contact, blocking
438 pollen hydration. As previously described, hydration appears as the first check point controlling
439 pollen rejection in SI species with dry stigma (Zuberi and Dickinson, 1985; Dickinson, 1995;
440 Samuel *et al.*, 2009; Hiroi *et al.*, 2013; Safavian and Goring, 2013; Wang *et al.*, 2016). In this
441 study, the hydration threshold required to trigger germination was found to correspond to a
442 pollen L/W ratio below 1.4. Pollen turgor pressure has been proposed to be the main driving
443 force for germination (Hiroi *et al.*, 2013; Vogler *et al.*, 2015; Wang *et al.*, 2016). Our result
444 indicates that the optimal pollen turgor pressure corresponds to a 1.4 L/W ratio which is
445 reached after 10 minutes of pollen deposition.
446 Although 19 % (10/53) of the incompatible grains exhibit hydration features similar to the
447 compatible ones, they, however, never germinate. Thus, a second check point acts to ensure
448 that undesirable pollen grains that escape the hydration control are properly inhibited, blocking
449 their germination. When hydration of incompatible pollen is artificially boosted in a saturated
450 humidity environment, a significant proportion of the grains bypasses the second checkpoint
451 and germinates. However, pollen tube growth is slow and does not reach the second phase of
452 rapid elongation observed with compatible tubes. Futhermore, tubes are abnormal, displaying
453 an enlarged extremity, and grow outside the papilla cell, unable to penetrate the cell wall.
454 Production of a short incompatible tube, whose growth is arrested in papilla cells, has been
455 described in some *S*-haplotypes of SI Brassica species (Elleman and Dickinson, 1994; Dickinson,

456 1995). Thus, our data highlight this late control of SI reaction that prevents penetration of the
457 stigmatic cell wall by incompatible tubes.
458
459 **Actin cytoskeleton**
460 In Brassica, remodeling of the actin cytoskeleton architecture has been described at the site of
461 pollen-stigma interaction (Iwano *et al.*, 2007). However, these results remain controversial, as a
462 previous work suggested that actin filaments do not show any rearrangement (Dearnaley *et al.*,
463 1999). Using an actin marker line, we show that a clear reorganization of actin occurs at the
464 contact site with compatible pollen. However, while actin bundles appear in Brassica papillae as
465 soon as pollen hydration starts and remain visible during the entire pollen hydration process
466 (Iwano *et al.*, 2007), in Arabidopsis, actin reorganization starts later, from the end of pollen
467 hydration and in most cases following pollen deformation or pollen tube emergence. One
468 explanation for these discrepancies could be that SI mechanism in Brassica and Arabidopsis
469 does not rely on rigorously similar cellular processes as previously proposed (Kitashiba *et al.*,
470 2011). Alternatively, these discrepancies could be due to technical reasons: (i) we used stable
471 transformed Arabidopis lines instead of transient expression in *Brassica* papillae, (ii) we
472 performed massive pollination of the stigmatic cells compared with deposition of a single
473 *Brassica* pollen by micromanipulation, and (iii) we used the Lifeact peptide instead of the mouse
474 Talin protein to label F-actin because this short peptide does not affect actin dynamics *in vivo*
475 (Era *et al.*, 2009). Nevertheless, whatever the species, actin focalization appears as a hallmark of
476 the compatible reaction as it is never detected in incompatible pollination. Interestingly,
477 Hardham et al. (2008) showed that touching the surface of the *A. thaliana* cotyledon epidermal
478 cells with a microneedle induced a rapid actin focalization around the contact point, leading the
479 authors to propose that actin reorganization is triggered by detection of mechanical pressure.
480 Likewise, reorganization of actin microfilaments was observed in many plant-pathogen
481 interactions, where actin cables accumulate at the contact site with the pathogen (Takemoto,
482 2004 and references therein). Altogether, we may hypothetize that reorganization of actin is
483 triggered in stigmatic cells that sense the mechanical pressure produced by the pollen
484 grain/tube at the site of cell wall penetration. In accordance with this, we generally did not

485 detect modification of the actin architecture at the contact site with incompatible pollen tubes
486 that were generated in high humidity conditions and that could not penetrate the stigmatic cell
487 wall. The focalization of actin at the pollen tube penetration site is also consistent with the well
488 characterized role of actin network in vesicular delivery to the plasma membrane (Szymanski
489 and Staiger, 2018). Indeed, the current SI model proposes that vesicular secretion is induced
490 upon compatible pollination to transport cargos required for stigmatic cell wall loosening and
491 pollen activation (reviewed in Jany *et al.*, 2019). Actin cables coud thus be involved in the
492 polarized secretion towards the pollen grain and the growing pollen tube.
493
494 Taking together, using fast scanning confocal microscopy, our observations underline the
495 suitability of our system to capture very dynamic events occurring within minutes. Notably, we
496 monitored the dynamics of actin network during compatible and incompatible responses and
497 found that focalization of actin cables was triggered when pollen-stigma interaction is engaged
498 in compatibility and elicited in response to mechanical pressure exerted by pollen grain/tube.
499
500 **Supplementary data**
501 **Protocol S1-S3**: supporting material
502 **Figure S1**: *AlSRK14* and *AlSCR14* Transgenic plant selection
503 **Video S1**: Dual pollination with compatible and incompatible pollen deposited on the same
504 stigma
505 **Video S2**: Actin rearrangement at the pollen contact site
506 **Video S3**: Actin rearrangement along the pollen tube path
507 **Video S4**: Actin behavior in stigmatic cells in contact with incompatible pollen
508 **Table S1**: L/W ratio of pollen grains coming out of mature anthers
509 **Figure S2**: Hydration kinetics of compatible and incompatible pollen in the semi *in vivo* system
510 **Table S2**: Germination of compatible pollen tracked during experiments described in figure 5
511 **Figure S3**: Standard and high humidity assays
512 **Figure S4**: Behavior of compatible pollen in high humidity conditions
513 **Video S5**: Compatible pollen germination and pollen tube growth in high humidity conditions

514 **Figure S5**: Behavior of incompatible pollen in high humidity conditions

515 **Table S3**: L/W ratio of incompatible pollen in high humidity conditions 10 minutes after pollen
516 deposition

517 **Video S6**: Incompatible pollen germination and pollen tube growth in high humidity conditions

518 **Figure S6**: FM4-64 labelling of stigmatic cells

519

520 **Acknowledgments**: We thank Fany Doustaly for *AlSRK14* transgenic line selection, Ghislaine
521 Laroche for *AlSCR14* construction and transgenic line selection, Annie Chaboud for giving us the
522 pAct11 and the pLat52 promoter regions and Claire Lionnet for her support with confocal
523 microscopy. We are grateful to Takashi Ueda for the *LifeActin:Venus* contruct and to Olivier
524 Haman for kindly giving us access to the confocal microscope (ERC-2013-CoG-615739). We thank
525 members of the SiCE team for fruitful discussions. This work was supported by CNRS and Grant
526 ANR-14-CE11-0021.

527

528 **References**

529 **Boggs NA, Dwyer KG, Nasrallah ME, Nasrallah JB**. 2009. In Vivo Detection of Residues Required
530 for Ligand-Selective Activation of the S-Locus Receptor in Arabidopsis. Current Biology **19**, 786–
531 791.

532 **Cabrillac D, Cock JM, Dumas C, Gaude T**. 2001. The S -locus receptor kinase is inhibited by
533 thioredoxins and activated by pollen coat proteins. Nature **410**, 220–223.

534 **Carter AL, McNeilly T**. 1976. Increased atmospheric humidity post pollination: A possible aid to
535 the production of inbred line seed from mature flowers in the Brussels sprout (Brassica oleracea
536 var. Gemmifera). Euphytica **25**, 531–538.

537 **Chapman LA, Goring DR**. 2010. Pollen-pistil interactions regulating successful fertilization in the
538 Brassicaceae. Journal of Experimental Botany **61**, 1987–1999.

539 **Cheung AY, Boavida LC, Aggarwal M, Wu H-M, Feijó JA**. 2010. The pollen tube journey in the
540 pistil and imaging the in vivo process by two-photon microscopy. Journal of Experimental
541 Botany **61**, 1907–1915.

542 **Dearnaley JDW, Clark KM, Heath IB, Lew RR, Goring DR**. 1999. Neither compatible nor self-
543 incompatible pollinations of Brassica napus involve reorganization of the papillar cytoskeleton.
544 New phytologist **141**, 199–207.

545 **Dickinson HG**. 1995. Dry stigmas, water and self-incompatibility in Brassica. Sexual Plant
546 Reproduction **8**, 1–10
547
548 **Doucet J, Lee HK, Goring DR**. 2016. Pollen Acceptance or Rejection: A Tale of Two Pathways.
549 Trends in Plant Science **21**, 1058–1067.

550 **Durand E, Meheust R, Soucaze M, *et al.*** 2014. Dominance hierarchy arising from the evolution
551 of a complex small RNA regulatory network. Science **346**, 1200–1205.

552 **Era A, Tominaga M, Ebine K, Awai C, Saito C, Ishizaki K, Yamato KT, Kohchi T, Nakano A, Ueda**
553 **T**. 2009. Application of Lifeact Reveals F-Actin Dynamics in Arabidopsis thaliana and the
554 Liverwort, Marchantia polymorpha. Plant and Cell Physiology **50**, 1041–1048.

555 **Elleman CJ, Dickinson HG**. 1994. Pollen-stigma interaction durmg self-incompatibility in *Brassica*
556 *oleracea.* In: Williams EG, Knox RB, Clarke AE. Genetic Control of Self-Incompatibility and
557 Reproductive Development in Flowering Plants. Netherlands: Kluwer, 67–87.
558
559 **Grebe M, Xu J, Möbius W, Ueda T, Nakano A, Geuze HJ, Rook MB, Scheres B**. 2003. Arabidopsis
560 sterol endocytosis involves actin-mediated trafficking via ARA6-positive early endosomes.
561 Current Biology **13**, 1378–1387.

562 **Hardham AR, Takemoto D, White RG**. 2008. Rapid and dynamic subcellular reorganization
563 following mechanical stimulation of Arabidopsis epidermal cells mimics responses to fungal and
564 oomycete attack. BMC Plant Biology **8**, 63.

565 **Hiroi K, Sone M, Sakazono S, Osaka M, Masuko-Suzuki H, Matsuda T, Suzuki G, Suwabe K,**
566 **Watanabe M**. 2013. Time-lapse imaging of self- and cross-pollinations in Brassica rapa. Annals
567 of Botany **112**, 115–122.

568 **Indriolo E, Safavian D, Goring DR**. 2014. The ARC1 E3 Ligase Promotes Two Different Self-Pollen
569 Avoidance Traits in Arabidopsis. The Plant Cell **26**, 1525–1543.

570 **Ivanov R, Fobis-Loisy I, Gaude T**. 2010. When no means no: guide to Brassicaceae self-
571 incompatibility. Trends in Plant Science **15**, 387–394.

572 **Iwano M, Shiba H, Miwa T, Che FS, Takayama S, Nagai T, Miyawaki A, Isogai A**. 2004. Ca2+
573 Dynamics in a Pollen Grain and Papilla Cell during Pollination of Arabidopsis. Plant Physiology
574 **136**, 3562–3571.

575 **Iwano M, Shiba H, Matoba K, *et al.*** 2007. Actin Dynamics in Papilla Cells of Brassica rapa during
576 Self- and Cross-Pollination. Plant Physiology **144**, 72–81.

577 **Jaillais Y, Fobis-Loisy I, Miège C, Gaude T**. 2007. Evidence for a sorting endosome in Arabidopsis
578 root cells: Plant sorting endosome. The Plant Journal **53**, 237–247.

579 **Jany E, Nelles H, Goring DR**. 2019. The Molecular and Cellular Regulation of Brassicaceae Self-
580 Incompatibility and Self-Pollen Rejection. International Review of Cell and Molecular Biology.
581 Elsevier, 1–35.

582 **Jelínková A, Malínská K, Simon S, *et al.*** 2010. Probing plant membranes with FM dyes: tracking,
583 dragging or blocking? The Plant Journal **61**, 883–892.

584 **Kandasamy MK, Nasrallah JB, Nasrallah ME**. 1994. Pollen-pistil interactions and developmental
585 regulation of pollen tube growth in Arabidopsis. Development **120**, 3405–3418.

586 **Kho YO, Baër J.** 1968. Observing pollen tubes by means of fluorescence. Euphytica 17, 298–302

587 **Kitashiba H, Liu P, Nishio T, Nasrallah JB, Nasrallah ME**. 2011. Functional test of Brassica self-
588 incompatibility modifiers in Arabidopsis thaliana. Proceedings of the National Academy of
589 Sciences **108**, 18173–18178.

590 **Lalonde BA, Nasrallah ME, Dwyer KG, Chen C-H, Barlow B, Nasrallah JB**. 1989. A highly
591 conserved Brassica gene with homology to the S-locus-specific glycoprotein structural gene. The
592 Plant Cell **1**, 249–258.

593 **Liu P, Sherman-Broyles S, Nasrallah ME, Nasrallah JB**. 2007. A Cryptic Modifier Causing
594 Transient Self-Incompatibility in Arabidopsis thaliana. Current Biology **17**, 734–740.

595 **Nasrallah ME**, **Nasrallah JB.** 2002. Generation of Self-Incompatible Arabidopsis thaliana by
596 Transfer of Two S Locus Genes from A. lyrata. Science **297**, 247–249.

597 **Nasrallah ME, Liu P, Sherman-Broyles S, Boggs NA, Nasrallah JB**. 2004. Natural variation in
598 expression of self-incompatibility in Arabidopsis thaliana: implications for the evolution of
599 selfing. Proceedings of the National Academy of Sciences of the United States of America **101**,
600 16070–16074.

601 **Nasrallah JB, Nasrallah ME**. 2014. *S* -locus receptor kinase signalling. Biochemical Society
602 Transactions **42**, 313–319.

603 **Nettancourt D de**. 2001. Incompatibility and Incongruity in Wild and Cultivated Plants. Berlin
604 Heidelberg: Springer-Verlag.

605 **Ockendon DJ**. 1978. Effect of hexane and humidity on self-incompatibility in Brassica oleracea.
606 Theoretical and Applied Genetics **52**, 113–117.

607 **Palanivelu R, Preuss D**. 2006. Distinct short-range ovule signals attract or repel Arabidopsis
608 thaliana pollen tubes in vitro. BMC Plant Biology **6**, 7.

609 **Safavian D, Goring DR**. 2013. Secretory Activity Is Rapidly Induced in Stigmatic Papillae by
610 Compatible Pollen, but Inhibited for Self-Incompatible Pollen in the Brassicaceae (D Bassham,
611 Ed.). PLoS ONE **8**, e84286.

612 **Samuel MA, Chong YT, Haasen KE, Aldea-Brydges MG, Stone SL, Goring DR**. 2009. Cellular
613 Pathways Regulating Responses to Compatible and Self-Incompatible Pollen in Brassica and
614 Arabidopsis Stigmas Intersect at Exo70A1, a Putative Component of the Exocyst Complex. THE
615 PLANT CELL ONLINE **21**, 2655–2671.

616 **Schopfer CR, Nasrallah ME, Nasrallah JB.** 1999. The Male Determinant of Self-Incompatibility in
617 Brassica. Science **286**, 1697–1700.

618 **Smyth DR, Bowman JL, Meyerowitz EM**. 1990. Early flower development in Arabidopsis. The
619 Plant Cell **2**, 755–767.

620 **Stein JC, Howlett B, Boyes DC, Nasrallah ME, Nasrallah JB**. 1991. Molecular cloning of a
621 putative receptor protein kinase gene encoded at the self-incompatibility locus of Brassica
622 oleracea. Proceedings of the National Academy of Sciences **88**, 8816–8820.

623 **Szymanski D, Staiger CJ**. 2018. The Actin Cytoskeleton: Functional Arrays for Cytoplasmic
624 Organization and Cell Shape Control. Plant Physiology **176**, 106–118.

625 **Takayama S, Shiba H, Iwano M, Shimosato H, Che F-S, Kai N, Watanabe M, Suzuki G, Hinata K,**
626 **Isogai A**. 2000. The pollen determinant of self-incompatibility in Brassica campestris.
627 Proceedings of the National Academy of Sciences **97**, 1920–1925.

628 **Takemoto D, Hardham AR.** 2004. The Cytoskeleton as a Regulator and Target of Biotic
629 Interactions in Plants. Plant Physiology **136**, 3864–3876.

630 **Tung CW, Dwyer KG, Nasrallah ME, Nasrallah JB.** 2005. Genome-Wide Identification of Genes
631 Expressed in Arabidopsis Pistils Specifically along the Path of Pollen Tube Growth. Plant
632 Physiology **138**, 977–989.

633 **Vogler F, Konrad SSA, Sprunck S**. 2015. Knockin' on pollen's door: live cell imaging of early
634 polarization events in germinating Arabidopsis pollen. Frontiers in Plant Science **6**.

635 **Wang L, Clarke LA, Eason RJ, Parker CC, Qi B, Scott RJ, Doughty J**. 2016. PCP-B class pollen coat
636 proteins are key regulators of the hydration checkpoint in *Arabidopsis thaliana* pollen-stigma
637 interactions. New Phytologist.

638 **Yang X, Zhang Q, Zhao K, Luo Q, Bao S, Liu H, Men S**. 2017. The Arabidopsis GPR1 Gene
639 Negatively Affects Pollen Germination, Pollen Tube Growth, and Gametophyte Senescence.
640 International Journal of Molecular Sciences **18**.

641 **Zuberi MI, Dickinson HG**. 1985. Pollen-stigma interaction in Brassica. III. Hydration of the pollen
642 grains. Journal of Cell Science **76**, 321–336.

643

644

645 **Figure Legends**

646

647 **Fig. 1.** Generation of SI Arabidopsis lines. (A) The Col-0 transgenic line expressing *AlSRK14* was
648 transformed with the fusion protein Act:Venus under the SLR1 promoter to label stigmas (green
649 fluorescence), whereas wild-type C24 or transgenic C24 expressing *AlSCR14* were transformed
650 with the TURQUOISE protein (TURQ, blue fluorescence) or the RFP protein (red fluorescence)
651 under pollen promoters, respectively. Bar = 20 μm. (B) SI phenotype of generated lines. Stage
652 13-14E stigmas were pollinated with mature pollen and pollen tubes present in stigmas were
653 counted after aniline blue staining. (C) Seed set. Stage 13-14E stigmas were pollinated with
654 mature pollen, after 21 days silique were dissected and seeds counted. n = number of pollinated
655 stigmas. Mean (black diamond) of 3 independent experiments. Black dots are extreme values.
656 Experiments separated by a dashed line were performed at different dates. Error bars indicate
657 SEM.

658

659 **Fig. 2.** Dynamics of the SI response in Col-0 background. (A) SI phenotype following pollination
660 of stigmas at two developmental stages. Flower buds at the end of developmental stage 12
661 were emasculated and pollinated with mature pollen 42h (stigma stage 15) or 66h (stigma stage
662 16) after emasculation (upper panel) and pollen tubes in stigmas were counted 6h after
663 pollination. Pollen tube count after aniline blue staining of stigmas (bottom graph). (B)
664 Maintenance of SI reaction over time. Flower buds at the end of stage 12 were emasculated,
665 pollinated with mature pollen 18h later (stage13-14) and harvested 6, 24, 48 or 72 hours after
666 pollination (upper panel). Pollen tube count after aniline blue staining of stigmas (bottom
667 graph). Beyond 100 pollen tubes per stigma, exact number was not determined and given a
668 value of 100 (no mean, no error bar for compatible crosses). n = number of pollinated stigmas.
669 Blue dots correspond to individual pollinated stigma; when several stigmas have the same
670 value, the stigma number is indicated in bracket. Mean (black diamond) of two independent
671 experiments. Black dots are extreme values. Error bars indicate SEM.

672

673 **Fig. 3.** Set up of the semi *in vivo* assay. (A) Distal portion of the pistil was cut (white line) and
674 stuck in a solid agar medium. To control humidity level, a small chamber made of a perforated
675 PCR tube, was placed on the medium. Stigma was pollinated and a coverslip was gently applied
676 for live imaging. Bar = 500 μm (B) Dual pollination on a single stigma. Stigma (Col-
677 0/SRK14+Act:Venus, green fluorescence) was pollinated first with incompatible pollen
678 (C24/SCR14+RFP, red fluorescence) and immediately after with compatible pollen (C24/TURQ,
679 blue fluorescence), and pollen behavior monitored under confocal microscopy for 32 minutes.
680 Image is a Z-projection (two minutes after pollen deposition). Bar = 50 μm. (C) Pollen
681 germination features extracted from 5 dual-pollinated stigmas. Only one incompatible grain
682 germinated (germination time = 28 min).
683
684 **Fig. 4**. Actin reorganization at the contact site with the compatible pollen grain and pollen tube.
685 (A) Visualization of actin bundles in unpollinated stigmatic cells expressing the Act:Venus marker
686 (Col-0/SRK14+Act:Venus, green fluorescence). Image is a Z-projection. (B) Dynamics of actin
687 focalization following compatible pollination. Act:Venus stigmas were dual-pollinated in the
688 semi *in vivo* system and a Z-stack was taken every minute during 32 minutes. Twenty four
689 Papillae in contact with a compatible pollen grain (blue fluorescence) were selected on 14
690 stigmas and first appearance of actin fluorescence (focalization) was recoved. Timing of actin
691 focalization was defined regarding the pollen development stage. (C) Actin reorganization in
692 papillae concomitant with pollen deformation. (D) Actin reorganization in papillae during
693 germination and pollen tube growth. Indicated time corresponds to time after pollen
694 deposition. Images are Z-projections. (E) Mutiple pollen germination on a single papilla. Image is
695 a Z-projection. Arrows show the focalization of actin fluorescence. Bar = 10 μm.
696
697 **Fig. 5.** Kinetics of compatible pollen hydration following dual pollination. (A) During hydration,
698 pollen shape changes from an ovoid towards a round shape given by the ratio Length/Width
699 (L/W). (B) Evolution of the L/W ratio during a compatible interaction. Among the 69 tracked
700 pollen grains, 58 germinated during the experiment (solid blue line), whereas 11 failed to
701 germinate (dashed blue line). (C) Kinetics of pollen hydration related to rate of germination.

702 Pollen grains were classified by their germination time in four categories: early, intermediate,
703 late and non germinated. Slopes were calculated by linear regression based on pollen hydration
704 curve during the first 10 minutes. n = number of pollen grains. Mean of five independent
705 experiments. Error bars indicate SEM.
706
707 **Fig. 6.** Kinetics of incompatible pollen hydration following dual pollination. (A) Evolution of the
708 L/W ratio during an incompatible interaction. Among the 53 tracked pollen grains, 43 exhibited
709 a L/W ratio that never reach the value of 1.4 (solid red line) whereas 10 had a ratio below 1.4
710 (dashed red line). The solid blue line that indicates hydration dynamics of compatibe pollen was
711 reproduced from Fig. 5B to facilitate the comparison.(B) hydration rates during the first 10
712 minutes of incompatible pollen with a L/W ratio >=1.4 (solid red line), incompatible pollen with
713 a L/W ratio <1.4 (dashed red line) and compatible pollen that lately germinated (solid blue line,
714 reproduced from Fig. 5C). Slopes were calculated by linear regression. n = number of pollen
715 grains. Mean of 5 independent experiments, error bars indicate SEM.
716
717 **Fig. 7.** Pollen germination in high humidity conditions. (A) Compatible pollen (blue fluorescence)
718 was deposited on an Act:Venus stigma and incubated in high humidity conditions. (B)
719 Incompatible pollen (red fluorescence) was deposited on an Act:Venus stigma and incubated in
720 high humidity conditions. A Z-stack was taken every minutes after pollen deposition. Images are
721 Z-projections. Bar = 10 μm. (C) Growth rate of pollen tubes in standard and high humidity
722 conditions. Pollen tube length was measured at each time point from germination (0 on the
723 horizontal axe) during 6 minutes, for compatible pollen developped in standard conditions (light
724 blue line), in high humidity conditions (dark blue line) or for incompatible pollen in high
725 humidity conditions (red line). n = number of tracked pollen grains on minimum 6 different
726 stigmas, error bars indicate SEM. (D) 35 minutes after incubation in high humidity conditions,
727 stigmas were stained with FM4-64 . A Z-stack was processed with image J to generate a 3D
728 projection. Compatible pollen tube (white star) was detected beneath the FM4-64 labelled layer
729 (red fluorescence surrounding the papilla cell), whereas incompatible tube (yellow star) was
730 outside. Bar = 10 μm.

Figure 1

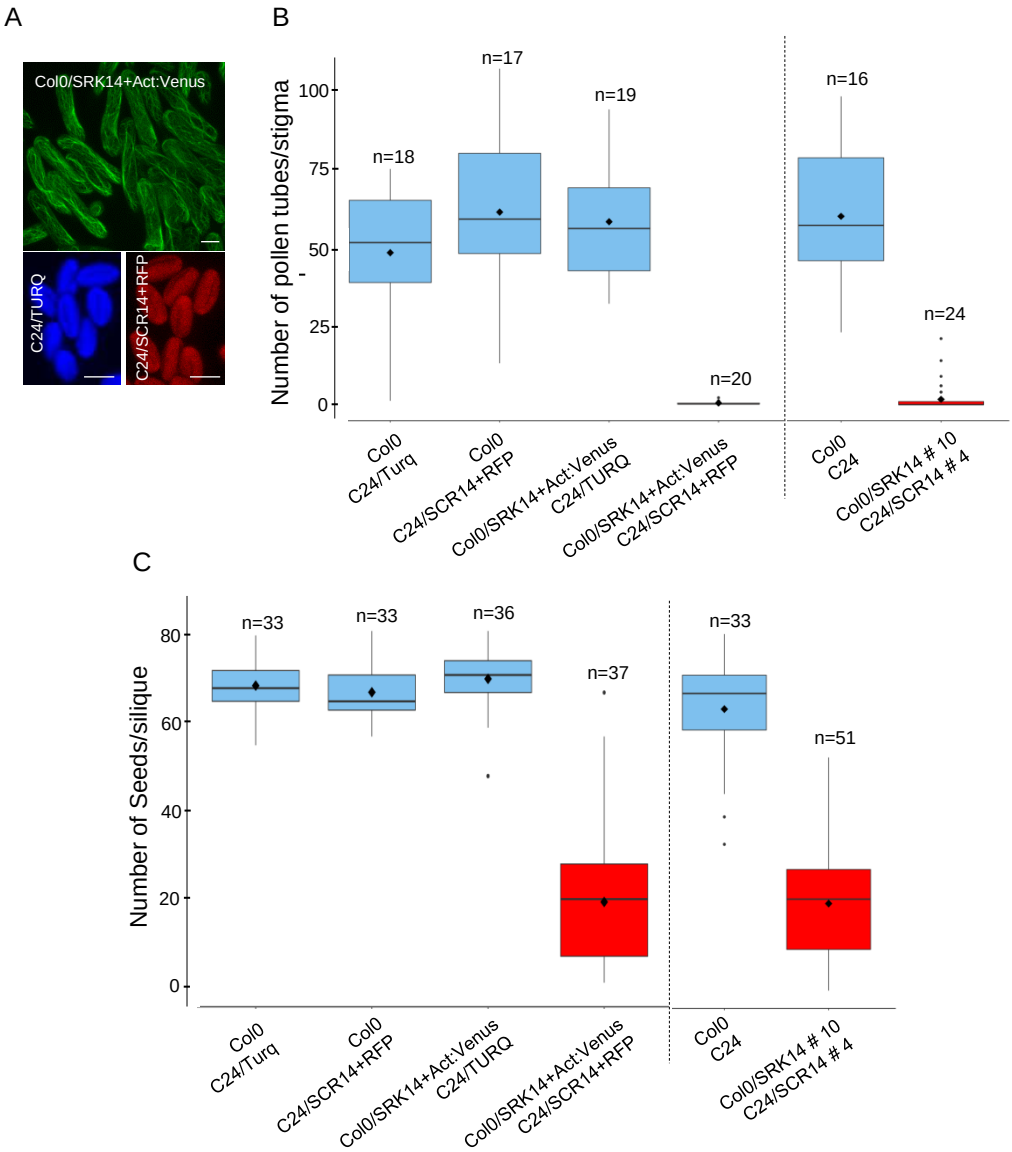
A
Col0/SRK14+Act:Venus
C24/TURQ
C24/SCR14+RFP
B
Number of pollen tubes/stigma
100
75
50
25
0
n=18
n=17
n=19
n=20
n=16
n=24
Col0
C24/Turq
Col0
C24/SCR14+RFP
Col0/SRK14+Act:Venus
C24/TURQ
Col0/SRK14+Act:Venus
C24/SCR14+RFP
Col0
C24
Col0/SRK14 # 10
C24/SCR14 # 4
C
Number of Seeds/silique
80
60
40
20
0
n=33
n=33
n=36
n=37
n=33
n=51
Col0
C24/Turq
Col0
C24/SCR14+RFP
Col0/SRK14+Act:Venus
C24/TURQ
Col0/SRK14+Act:Venus
C24/SCR14+RFP
Col0
C24
Col0/SRK14 # 10
C24/SCR14 # 4

Figure 2

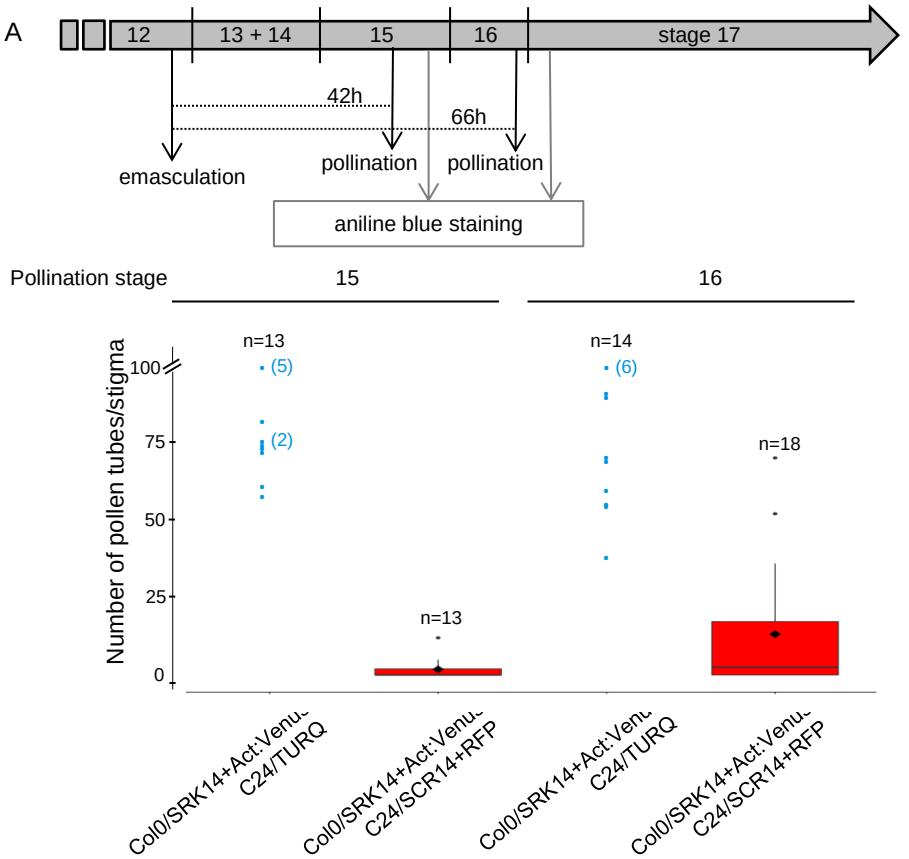
A
12
13 + 14
15
16
stage 17
42h
66h
emasculation
pollination
pollination
aniline blue staining
Pollination stage
15
16
Number of pollen tubes/stigma
100
75
50
25
0
n=13
(5)
(2)
n=13
n=14
(6)
n=18
Col0/SRK14+Act:Venus C24/TURQ
Col0/SRK14+Act:Venus C24/SCR14+RFP
Col0/SRK14+Act:Venus C24/TURQ
Col0/SRK14+Act:Venus C24/SCR14+RFP

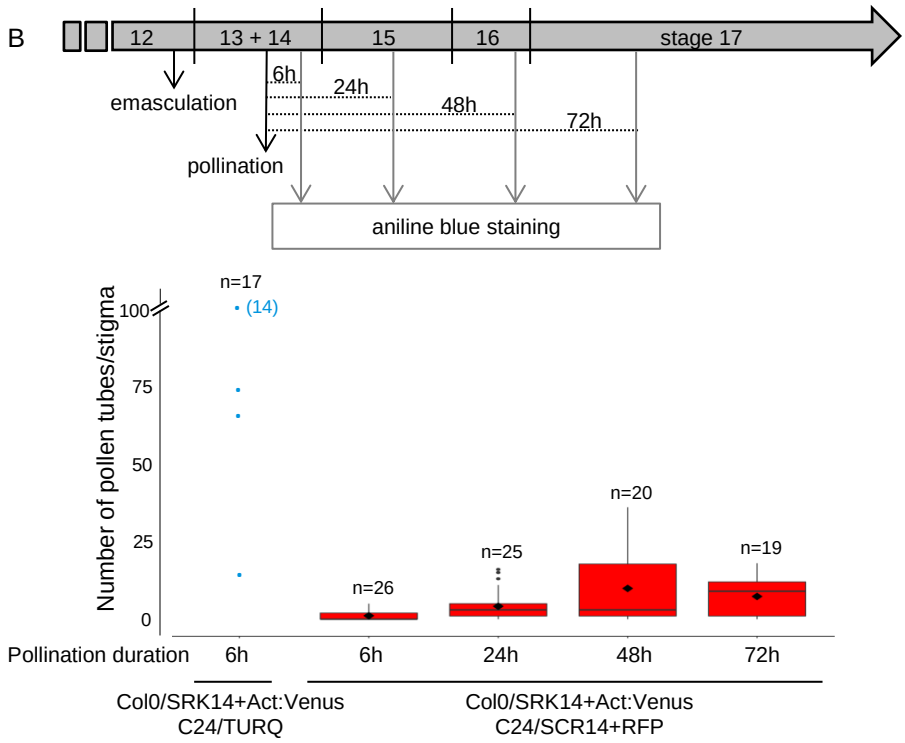
B
12
13 + 14
15
16
stage 17
emasculation
6h
24h
48h
72h
pollination
aniline blue staining
Number of pollen tubes/stigma
100
75
50
25
0
n=17
(14)
n=26
n=25
n=20
n=19
Pollination duration
6h
6h
24h
48h
72h
Col0/SRK14+Act:Venus C24/TURQ
Col0/SRK14+Act:Venus C24/SCR14+RFP

Figure 3

A

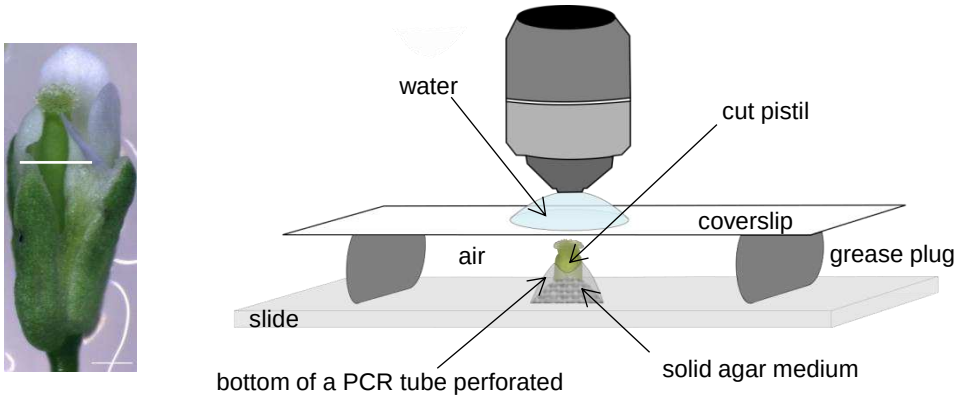

B

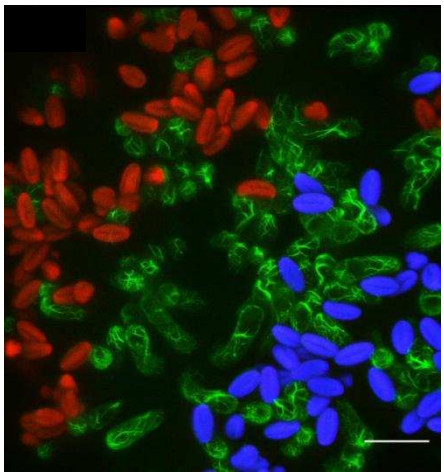

C

	germination			pollen number
	%	time (min)	SEM	
compatible	74	20.38	0.55	106
incompatible	1.3	-	-	75

Figure 4

A

B

first appearance of actin focalization in papilla	number of papilla
before pollen deformation	6/24 (25%)
concomitant with pollen deformation	4/24 (17%)
concomitant with pollen tube emergence	2/24 (8%)
just after germination	10/24 (42%)
no actin focalization	2/24 (8%)

C

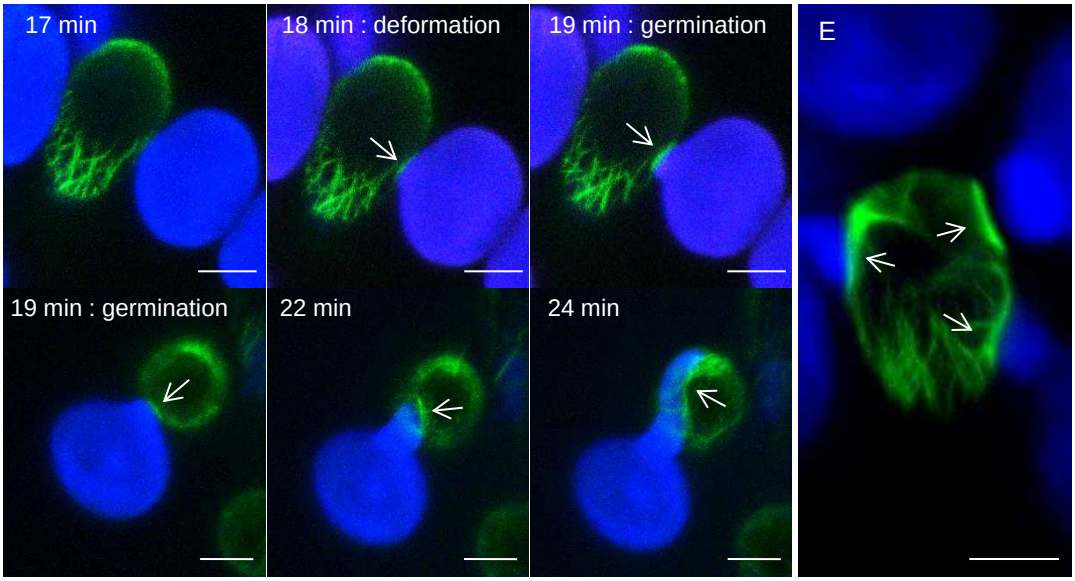

D

Figure 5

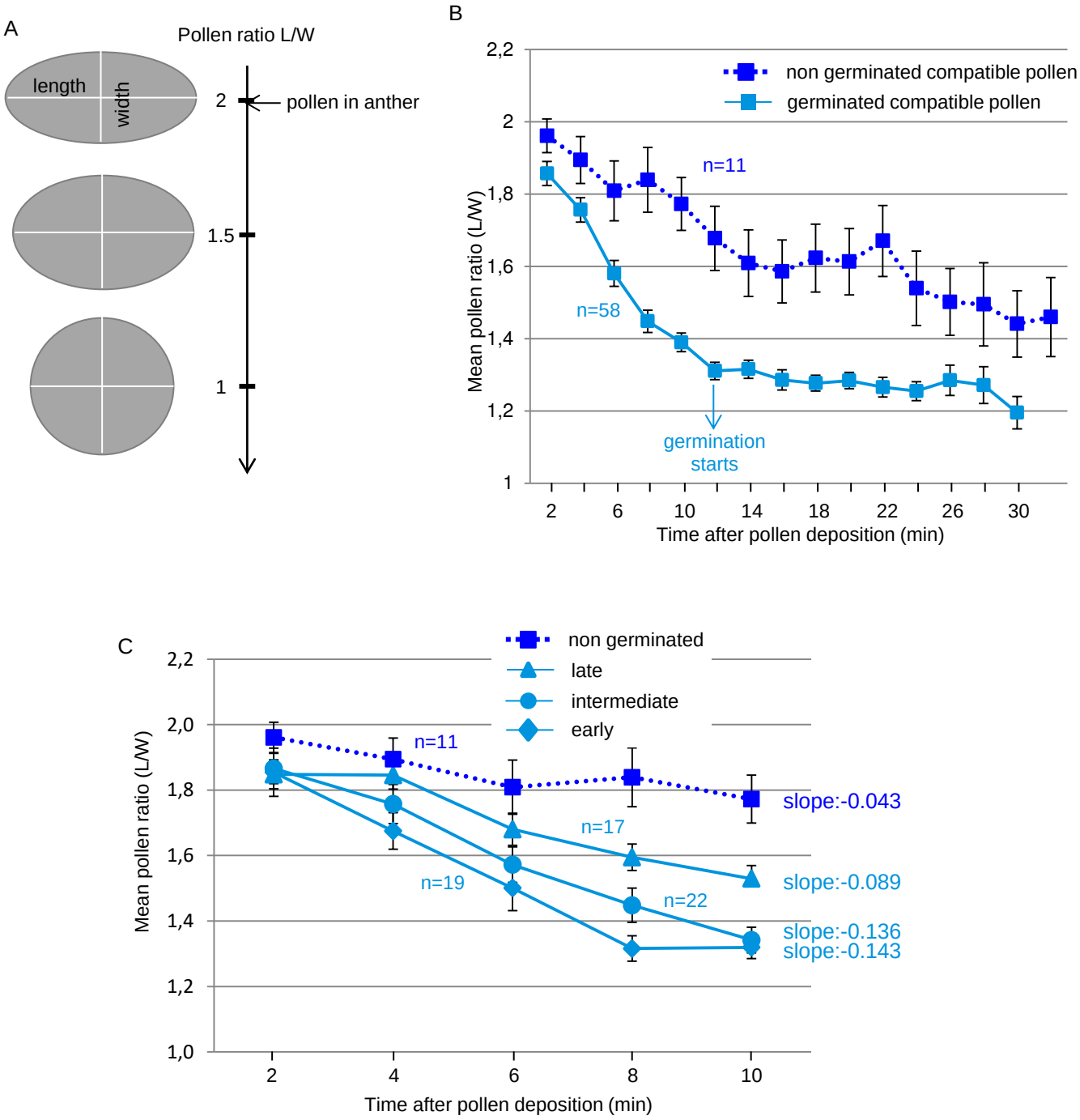
A
Pollen ratio L/W
length
width
2
pollen in anther
1.5
1
B
non germinated compatible pollen
germinated compatible pollen
n=11
n=58
germination starts
Mean pollen ratio (L/W)
Time after pollen deposition (min)
C
non germinated
late
intermediate
early
n=11
n=17
n=19
n=22
slope:-0.043
slope:-0.089
slope:-0.136
slope:-0.143
Mean pollen ratio (L/W)
Time after pollen deposition (min)

Figure 6

A

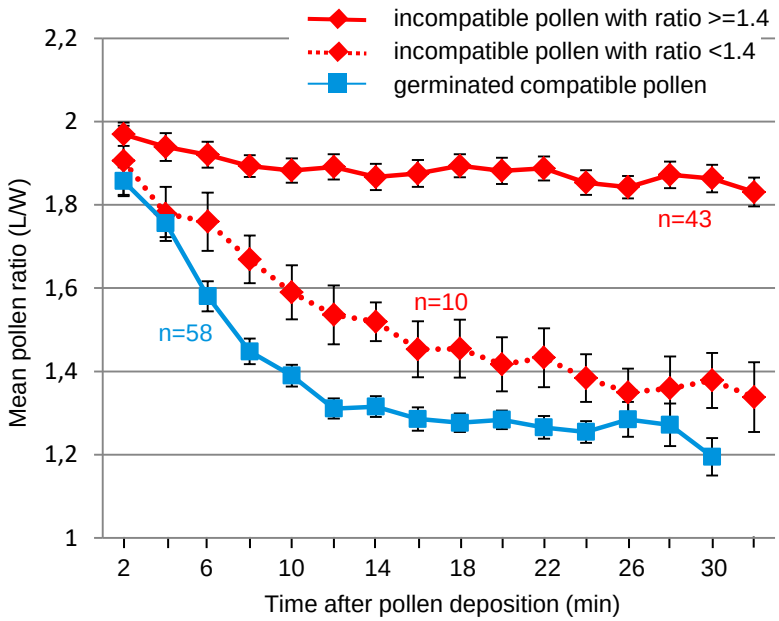
incompatible pollen with ratio >=1.4
incompatible pollen with ratio <1.4
germinated compatible pollen
Mean pollen ratio (L/W)
2,2
2
1,8
1,6
1,4
1,2
1
2
6
10
14
18
22
26
30
Time after pollen deposition (min)
n=43
n=10
n=58

B

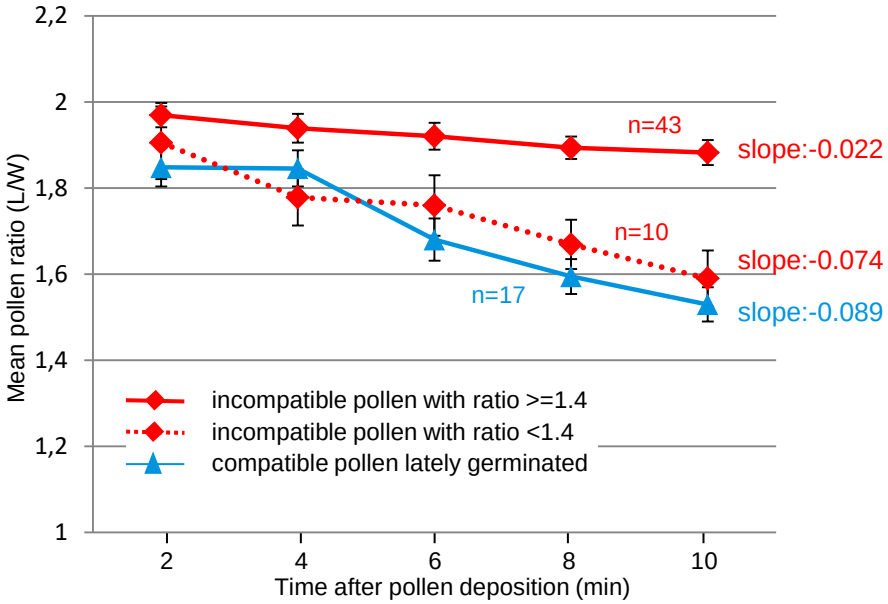
Mean pollen ratio (L/W)
2,2
2
1,8
1,6
1,4
1,2
1
2
4
6
8
10
Time after pollen deposition (min)
n=43
slope:-0.022
n=10
slope:-0.074
n=17
slope:-0.089
incompatible pollen with ratio >=1.4
incompatible pollen with ratio <1.4
compatible pollen lately germinated

Figure 7

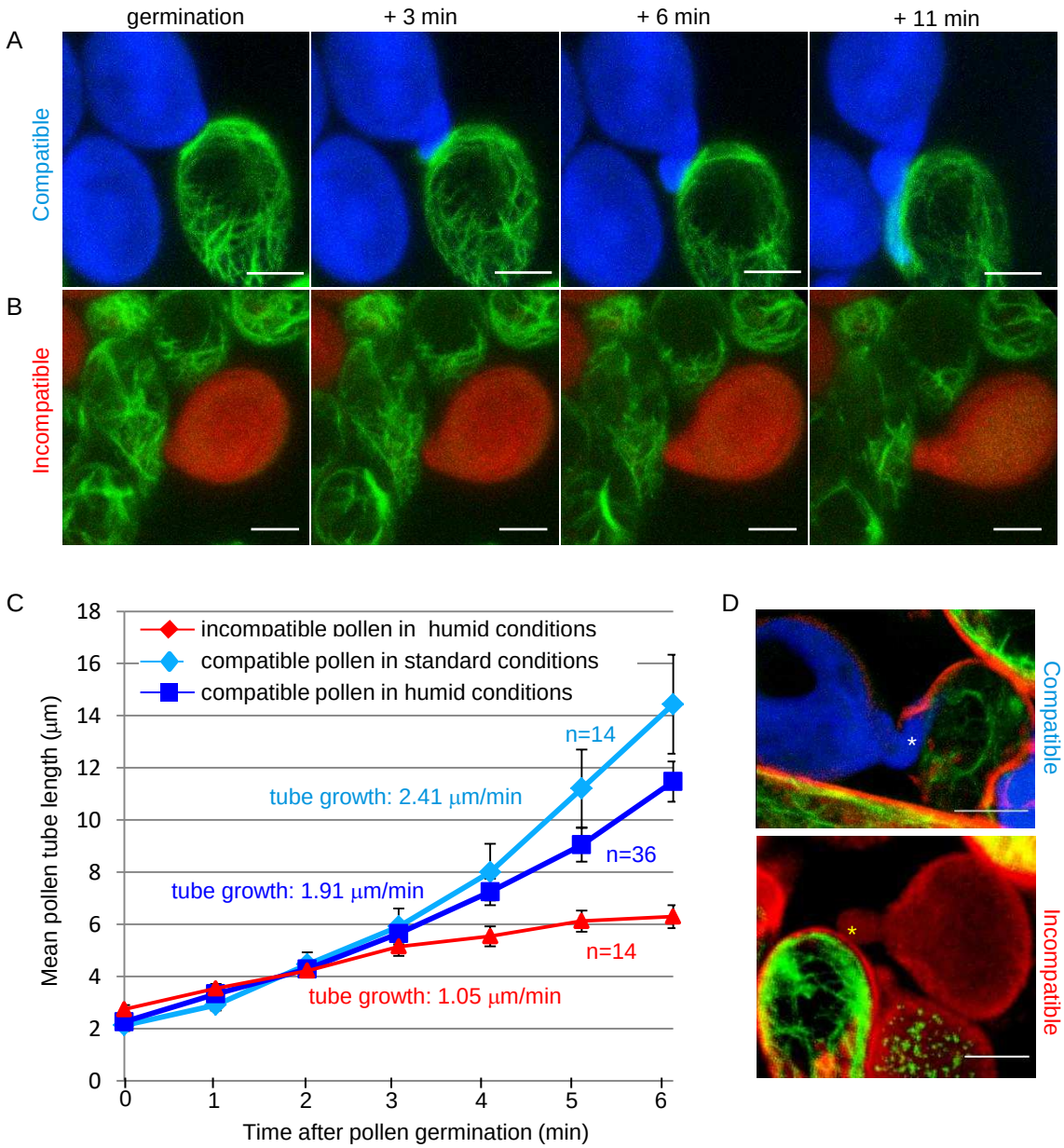
germination
+ 3 min
+ 6 min
+ 11 min
A
Compatible
B
Incompatible
C
incompatible pollen in humid conditions
compatible pollen in standard conditions
compatible pollen in humid conditions
n=14
tube growth: 2.41 µm/min
n=36
tube growth: 1.91 µm/min
n=14
tube growth: 1.05 µm/min
Mean pollen tube length (µm)
Time after pollen germination (min)
0
2
4
6
8
10
12
14
16
18
0
1
2
3
4
5
6
D
Compatible
Incompatible